Eurasian Journal of Physics and Functional Materials

2020, 4(1), 19-28

Neutron transfer and nuclear breakup in ^{208}Pb(^{11}Li,^{9}Li) reaction

A.K. Azhibekov*[,1,2], V.V. Samarin[2,3], K.A. Kuterbekov[1]

[1]L.N. Gumilyov Eurasian National University, Nur-Sultan, Kazakhstan

[2]Joint Institute for Nuclear Research, Dubna, Russia

[3]Dubna State University, Dubna, Russia

E-mail: azhibekoaidos@mail.ru

DOI: **10.29317/ejpfm.2020040103**
Received: 14.01.2020 - after revision

Neutron transfer and nuclear breakup processes in reaction with weakly bound nucleus ^{11}Li at energies near the Coulomb barrier are investigated in the framework of the time-dependent Schrödinger equation. The evolution of probability density of outer weakly bound neutrons of ^{11}Li in the collision with ^{208}Pb was studied. The probabilities and cross sections of outer neutrons removal (breakup processes and transfer to target nucleus) were calculated. Theoretical predictions of the two-neutron removal probability values were obtained for angles from 140° to 180°. The theoretical results have close similarity with experimental data for the two-neutron removal in reaction ^{208}Pb(^{11}Li,^{9}Li).

Keywords: time-dependent Schrödinger equation; neutron transfer and breakup reactions; weakly bound nuclei.

Introduction

The latest experimental data on elastic scattering of light weakly bound lithium nuclei ^{8,9,11}Li indicates enhancement of the total cross section for reactions with these nuclei as compared to reactions with ^{6,7}Li [1-6]. This effect is especially strongly manifested for light nuclei with a neutron halo [7]. So-called halo nuclei with broad distribution of weakly bound nucleons are studied more than twenty years, e.g. see [8, 9]. Our previous work [10] was devoted to investigation neutron transfer and nuclear breakup processes in ^{11}Li + ^{9}Be and ^{11}Li + ^{12}C reactions at low energies in the framework of the time-dependent Schrödinger equation. In

this approach we carry out a theoretical description of the experimental data on direct nuclear reactions of the weakly bound ^{11}Li halo nucleus with a heavy ^{208}Pb target at near barrier energies. The experimental data described in this paper were obtained by the authors of [11, 12] at the TRIUMF facility (Vancouver, Canada).

Theory and numerical methods

The structure of the ^{11}Li projectile nucleus and the ^{208}Pb target nucleus described in framework the shell model of a spherical nucleus without spin-orbit interaction, as in [10]. Taking into account spin-orbit interaction in the used approach does not lead to essential distinctions in the results, see [13]. The ^{208}Pb nucleus has a slight deformation with parameter quadruple deformation $\beta_2 = 0.0544$. It confirms the possibility of application of the spherical shell model to description ^{208}Pb nucleus. The results of calculations of single-particle energy levels of neutrons are presented in Figure 1. The three parameters of the Woods-Saxon potential of the mean field are the radius $R^{\mathrm{WS}} = r^{\mathrm{WS}}A^{1/3}$, the diffuseness a^{WS} and the depth V^{WS} of potential well. For both nuclei the "universal" values of r^{WS} (1.347 fm) and a^{WS} (0.7 fm) were chosen from [14], and potential depth V^{WS} was varied. For neutron in the topmost occupied level the separation energy is equal to experimental value 7.37 MeV for ^{208}Pb nucleus and 0.396 MeV for ^{11}Li nucleus.

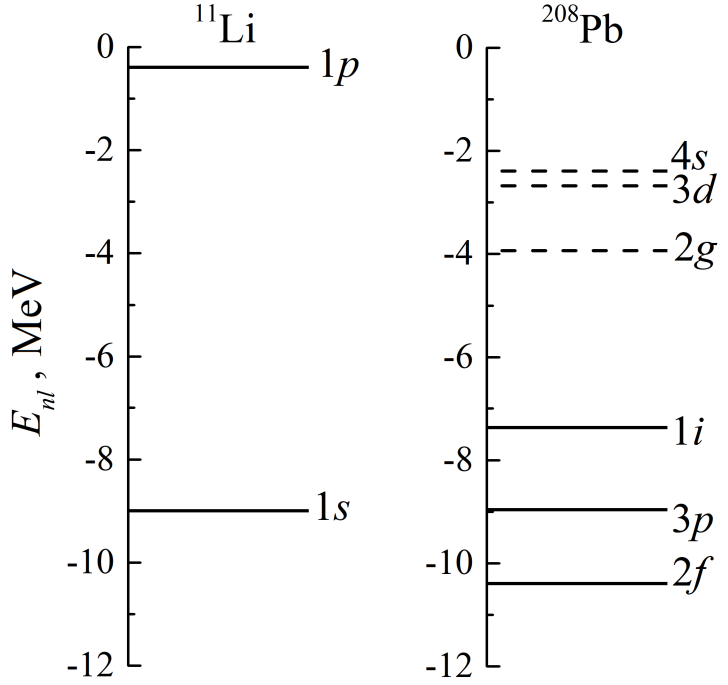

Figure 1. Single-particle neutron energy levels in the ^{11}Li nucleus and upper levels in the ^{208}Pb nucleus in shell models without spin-orbit interaction.

The normalized radial wave functions $R_{nl}(r)$ for the neutron levels are shown in Figure 2. The radial wave functions $R_{nl}(r)$ were calculated by integration from large values of radius to small values, see e.g. [15, 16].

The normalization condition for all radial wave functions was

$$\int_0^{r_{max}} R_{nl}^2 r^2 dr = 1 \tag{1}$$

where the upper bound r_{max} was equal to 40 fm. For optimization of calculations we reduced the upper bound $r_b < r_{max}$, the values of r_b and $1 - J << 1$ with integral J

$$J = \int_0^{r_b} R_{nl}^2 r^2 dr \tag{2}$$

are given in Table 1. The values r_b may be considered as the bounds of the neutron distributions ("clouds").

Table 1.
The bounds r_b of the neutron distributions and the values of $1 - J$ for normalization integral (2).

Nucleus	^{11}Li	^{208}Pb					
r_b , fm	20	15					
Level	*1p*	*2f*	*3p*	*1i*	*2g*	*3d*	*4s*
$1 - J$	$2 \cdot 10^{-3}$	$4.6 \cdot 10^{-6}$	$3 \cdot 10^{-5}$	$2 \cdot 10^{-6}$	$1.5 \cdot 10^{-4}$	$2 \cdot 10^{-3}$	$2 \cdot 10^{-3}$

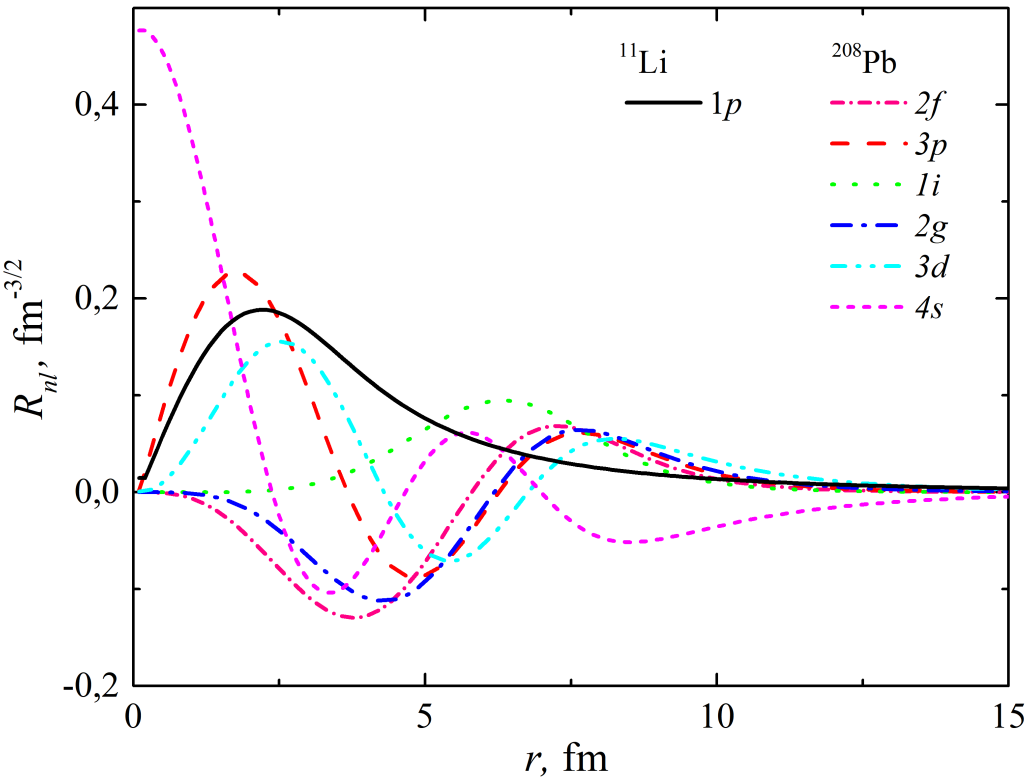

Figure 2. Radial part $R_{nl}(r)$ of the wave functions for neutron levels of the ^{11}Li and ^{208}Pb nuclei in the shell model without spin-orbit interaction.

In the central field of the nucleus the wave functions of the neutron with certain values of the orbital moment l and its projection on the z axis are equal to $\psi_{nlm_l}(r,\theta,\varphi) = R_{nl}(r)Y_{lm_l}(\theta,\varphi)$, here Y_{lm} are spherical harmonics.

Evolution of wave function of outer neutron in field of colliding nuclei is described by the time-dependent Schrödinger equation (TDSE)

$$i\hbar\frac{\partial\Psi}{\partial t} = -\frac{\hbar^2}{2m}\Delta\Psi + V\left(\vec{r};\vec{r}_1(t),\vec{r}_2(t)\right)\Psi \tag{3}$$

Here $\vec{r}_1(t)$, $\vec{r}_2(t)$ are the radius-vectors of the centers of the colliding nuclei with masses m_1 and m_2, which moved along classical trajectories. The equations of classical mechanics for colliding nuclei have the form:

$$m_1\ddot{\vec{r}}_1 = -\nabla_{r_1}V_{12}(\left|\vec{r}_1-\vec{r}_2\right|), m_2\ddot{\vec{r}}_2 = -\nabla_{r_2}V_{12}(\left|\vec{r}_1-\vec{r}_2\right|) \tag{4}$$

where $V_{12}(r)$ is the nucleus-nucleus potential in the Akyuz-Winther form [17]. The well-known fourth-order Runge–Kutta method of the Cauchy problem for ordinary differential equations was used for numerical solving Eq. (4) in combination with numerical solving Eq. (3) in the center of mass system. TDSE is solved iteratively in time with the fast complex Fourier transform [18] on a spatial grid with a plane of symmetry (the collision plane). A detailed description of the solution of the equation without spin-orbit interaction for nuclear reactions is presented in our previous work [10]. The lattice spacing in the TDSE calculation is 0.3 fm, which is substantially smaller than 0.8 fm in a typical time-dependent Hartree-Fock calculation [19]. The colliding nuclei are en-closed in a box of typical dimensions $105\times105\times130$ fm^3.

The initial conditions $\Psi(\vec{r},t=0)$ for numerical solving of the time-dependent Schrödinger equation is the wave function of stationary state ψ_{nlm} in the moving projectile nucleus

$$\Psi(\vec{r},t=0) = \psi_{nlm}(\vec{r}-\vec{r}_{10})\exp\left(i\frac{m\vec{v}_{10}\vec{r}}{\hbar}\right) \tag{5}$$

here $\vec{v}_{10}$ is velocity of ^{11}Li nucleus in the initial point $\vec{r}_{10}$ in the center of mass system.

The scattering angles in the center of mass system were calculated by numerical simulations for large times when the nucleus-nucleus interaction potential can be neglected. The scattering angle $\theta_{\text{c.m.}}$ in the center of mass system is equal to the rotation angle of the velocity vector

$$\theta_{\text{c.m.}} = \begin{cases} \operatorname{sgn}(v_x)\frac{\pi}{2}, & \text{if} \quad v_z = 0 \\ \pi, & \text{if} \quad v_x = 0,\ v_z > 0 \\ 0, & \text{if} \quad v_x = 0,\ v_z < 0 \\ \arctan\left(-\frac{v_x}{v_z}\right), & \text{if} \quad v_z < 0, \\ \pi - \arctan\left(\frac{v_x}{v_z}\right), & \text{if} \quad v_z > 0, \quad v_x > 0, \\ -\pi - \arctan\left(\frac{v_x}{v_z}\right), & \text{if} \quad v_z > 0, \quad v_x < 0, \end{cases} \tag{6}$$

where v_x, v_z – the projection of the projectile velocity vector calculated by equation (4). To relate the angles between the in the center-of-mass $\theta_{\text{c.m.}}$ and laboratory

frames θ_{lab} following equation was used

$$\tan\theta_{\text{lab}} = \frac{\sin\theta_{\text{c.m.}}}{\cos\theta_{\text{c.m.}} + m_1/m_2} \tag{7}$$

Results of calculations

To verify the accuracy of the TDSE solutions, the probability of the neutron remaining in the ^{11}Li nucleus during the free motion of ^{11}Li at an energy of 24.3 MeV was calculated. The probability that the neutron remained in the projectile nucleus ^{11}Li can be calculated as an integral over the region S_1, which is a sphere with a center at $\vec{r}_1(t)$ and a radius $r_1 = 20$ fm (see Table 1)

$$p_{\text{r}} = \int_{S_1} |\Psi|^2 \, dV \tag{8}$$

At the end of the movement of the ^{11}Li nucleus to a distance of 85 fm, the value of the integral (8) was 0.99528. The lost probability determines the error of the numerical solution of the Schrödinger equation equal to 0.47%. The errors of the calculations are depended on the lattice spacing. It is possible to reduce the error by several orders of magnitude by reducing the lattice spacing, but this will lead to an increase in the number of nodes and counting time. Therefore, to optimize the computational processes, a grid step was selected with an allowable error of less than 0.5%. The evolution of the probability density of an outer neutron during free motion of the ^{11}Li nucleus is shown in Figure 3. It can be seen that the probability density does not change over time.

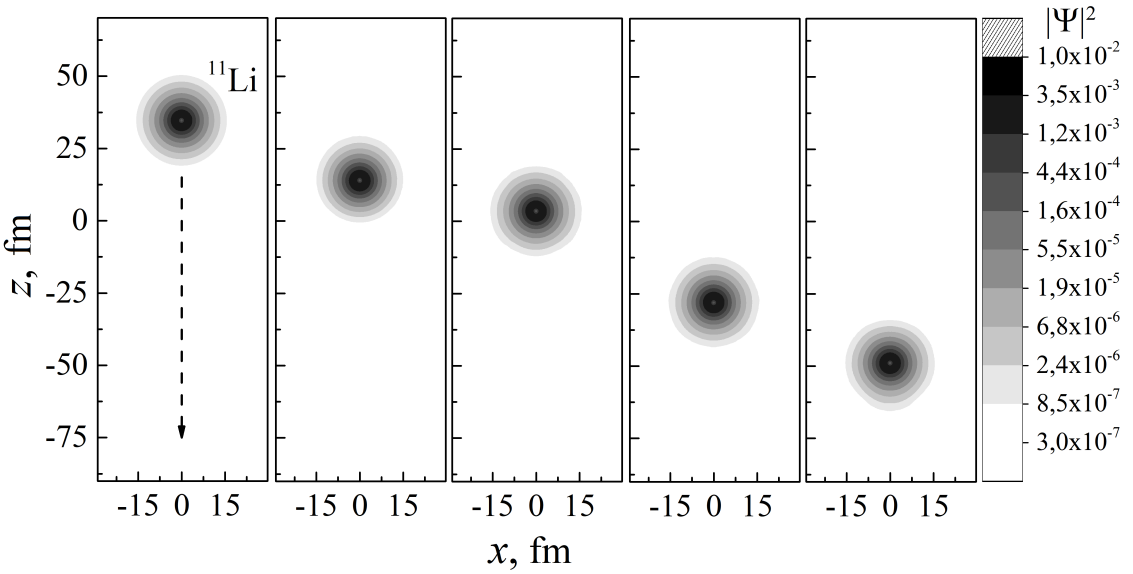

Figure 3. Evolution of probability density of outer neutron of ^{11}Li during the free motion of nucleus. Time scale is from left to right. Gradient scale is logarithmic.

The Coulomb barrier for central collision ^{11}Li + ^{208}Pb is equal to 28.51 MeV for nucleus-nucleus potential in the Akyuz-Winther form [16]. The evolution of the probability density of outer neutron of the ^{11}Li nucleus in collisions with the ^{208}Pb

nucleus at energies of 24.3 and 29.8 MeV (these energies in the center-of-mass frame are equal to 23.1 and 28.3 MeV, respectively) is shown in Figures 4 and 5. It can be seen, the TDSE solution allowed us to visualize the dynamics of the processes taking place. At the close distance between the colliding nuclei the outer neutrons of ^{11}Li nucleus are collectivized and common neutron "cloud" is formed (panels b, f in Figures 4 and 5). When the nuclei move away from each other neutron "cloud" is divided into three parts (panels c, d, g, h in Figures 4 and 5). First part is neutron "cloud" remaining in projectile nucleus ^{11}Li and second part is neutron "cloud" transferred into states of target nucleus unoccupied by other neutrons. Third part corresponds to free neutrons in states of continuum energy spectrum (breakup of ^{11}Li nucleus to $^{10}\mathrm{Li} + n$).

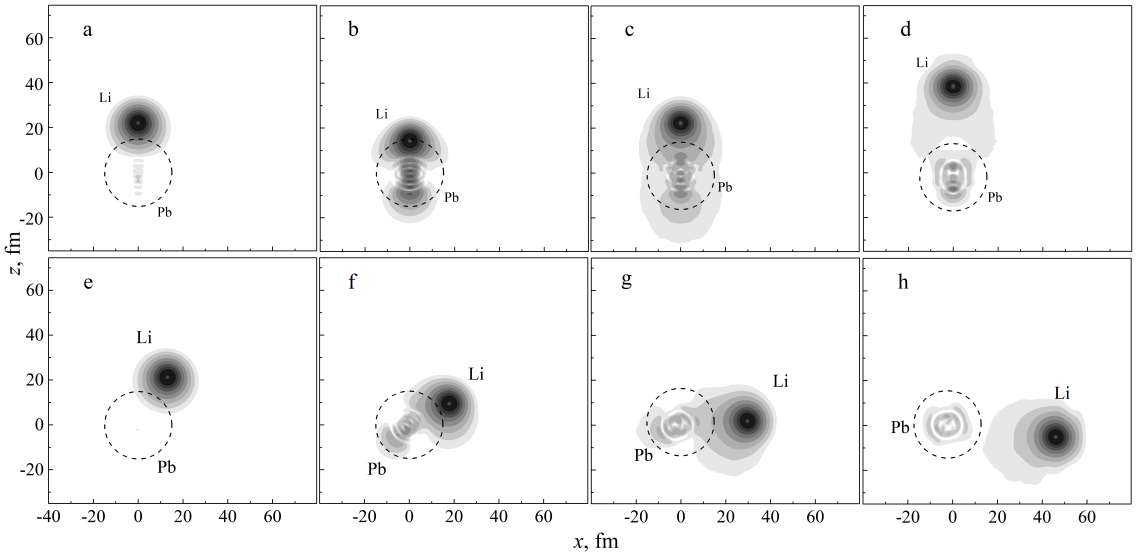

Figure 4. Evolution of probability density of outer neutron of ^{11}Li for central collision (a-d) and for grazing collision (e-h) with 208Pb at E = 24.3 MeV ($E_{\mathrm{c.m.}}$ = 23.1 MeV) and impact parameters b = 0 and b = 12 fm. Time scale is from left to right.

During the grazing collisions of nuclei the transfer probability of one outer neutron may be determined as

$$p_{\mathrm{tr}} = \int_{S_2} |\Psi|^2 \, dV \tag{9}$$

where S_2 is a sphere with a center at and a radius r_2 = 15 fm (see Table 1). As can be seen from panels d, h in Figures 4 and 5 the neutron transfer process is more intensive for collision at energy of 29.8 MeV ($E_{\mathrm{c.m.}}$ = 28.3 MeV), this energy is closer to the Coulomb barrier 28.5 MeV.

The transfer process was accompanied by the transition of the neutron to the continuum state, i.e. the breakup of the projectile. The probability of breakup

$$p_{\mathrm{br}} = C \cdot (1 - p_{\mathrm{tr}} - p_{\mathrm{r}}) \tag{10}$$

where C is a variable (adjustable) parameter. Parameter C was introduced to take account of slowly transition of neutron to states of continuum spectrum (panels c, d, g, h in Figures 4 and 5). It is assumed that the released neutrons initially appear in the peripheral region of the target nucleus in the form of a compact

three-dimensional wave packet and then gradually leave it when the packet spreads. Our calculations with C = 1.5 gives close similarity with experimental data.

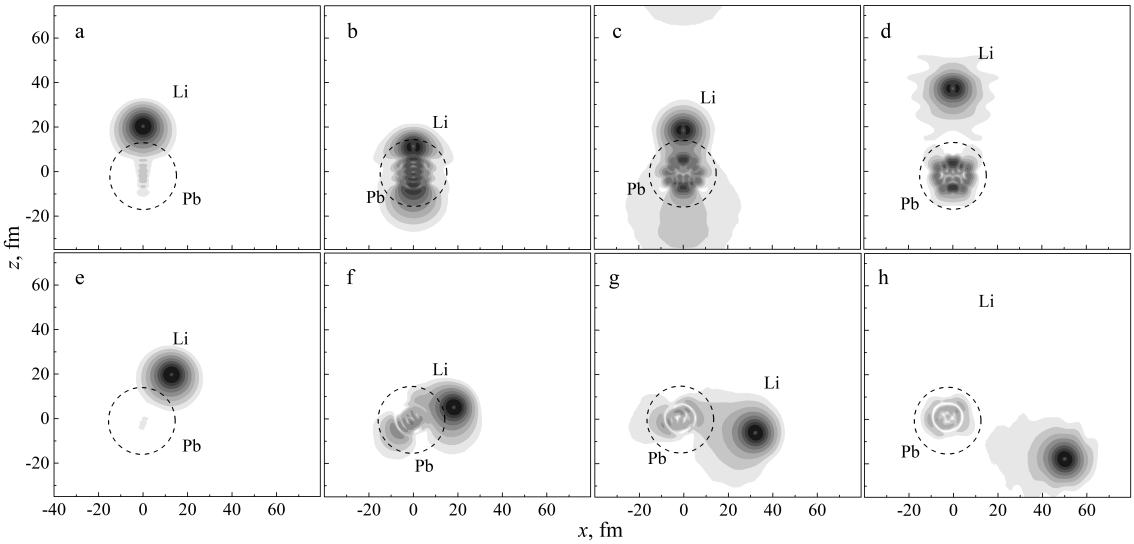

Figure 5. Evolution of probability density of outer neutron of ^{11}Li for central collision (a-d) and for grazing collision (e-h) with ^{208} Pb at E=29.8 MeV ($E_{\text{c.m.}}$ =28.3 MeV) and impact parameters b=0 and b=12 fm. Time scale is from left to right.

The ^{11}Li nucleus is an excellent example of the so-called Borromeo system, in which none of the two-particle subsystems ($^{9}\text{Li} + n$, $n + n$) forms a bound state. The removal of the one neutron leads to the breakup of the ^{10}Li nucleus to n and the ^{9}Li nucleus. In our calculations the two-neutron removal probabilities in reaction (^{11}Li, ^{9}Li) was determined by

$$p_{-2n} = 1 - (1 - p_{\text{tr}} - p_{\text{br}})^2 \tag{11}$$

The neutron transfer to the unoccupied bound states of the discrete spectrum in the ^{208}Pb nucleus, the probabilities of transfer to the states of the continuous spectrum (nuclear breakup) and the two-neutron removal probabilities as functions of distance of the closest approach $R_{\text{min}}(b, E)$ are shown in Figure 6.

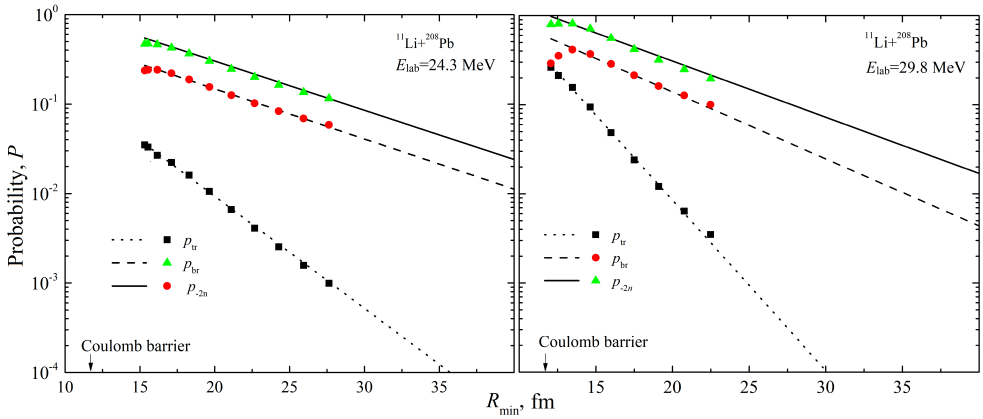

Figure 6. The neutron transfer (p_{tr}) to the unoccupied bound states of the discrete spectrum in the ^{208}Pb nucleus, the transfer to the states of the continuous spectrum (p_{br}) and the two-neutron removal (p_{-2n}) probabilities as functions of the distance of the closest approach $R_{\text{min}}(b, E)$.

The experimental values of the two-neutron removal probabilities in collisions of ^{11}Li with ^{208}Pb nucleus at energies of 24.3 and 29.8 MeV shown in Figure 7

were determined as the ratio of ^{9}Li events to the sum of ^{9}Li and ^{11}Li events for a given scattering angle [11]. Note that, according to experimental data, the high yield of ^{9}Li at backward angles is comparable with the yield of ^{11}Li at 24.3 MeV and 70% more at 29.8 MeV. Calculations indicate that at 29.8 MeV, the ^{9}Li yield is greater due to the greater probability of neutron transfer to the target. As can be seen from the Figure 7, theoretical calculations describe the experimental data values gradually increase with increasing angle. Moreover, theoretical predictions of probability values are obtained for angles from 140° to 180°. It should be noted that one of the advantages over other models of nuclear reactions is that TDSE approach allow us to calculate with good accuracy the probabilities of the channels neutron transfer and nuclear breakup.

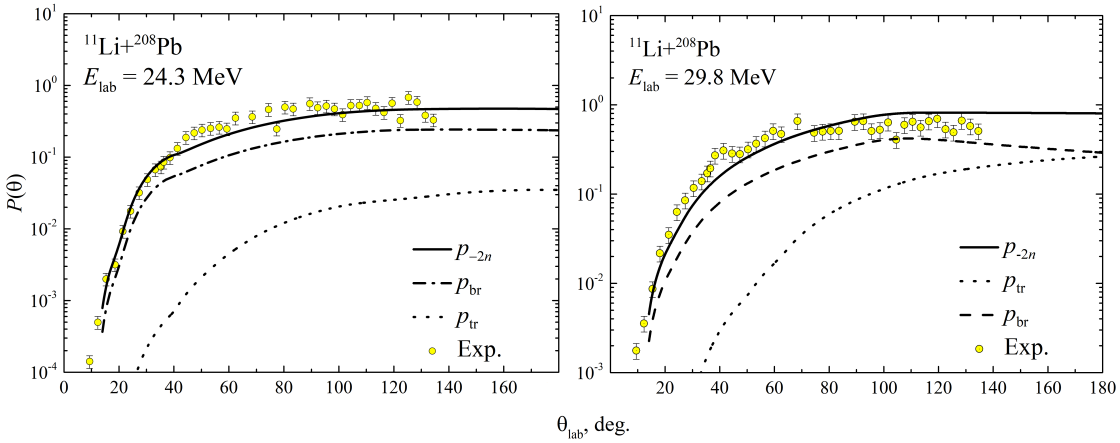

Figure 7. The neutron transfer (p_{tr}) to the unoccupied bound states of the discrete spectrum in the ^{208}Pb nucleus, the transfer to the states of the continuous spectrum (p_{br}) and the two-neutron removal (p_{-2n}) probabilities angular distributions, in the laboratory frame, for the reaction ^{11}Li + ^{208}Pb . The circles represent the experimental data [11].

The cross-sections for two-neutron removal σ_{-2n} and neutron transfer σ_{tr} channels are obtained by integrating over the impact parameter b

$$\sigma_{-2n}(E) = 2\pi \int_{b_{\min}}^{\infty} p_{-2n}(R_{\min}(b,E))bdb \tag{12}$$

$$\sigma_{\text{tr}}(E) = 2\pi \int_{b_{\min}}^{\infty} p_{\text{tr}}(R_{\min}(b,E))bdb \tag{13}$$

where $b_{\min}$ corresponds to $R_{\min} = 1.2 \cdot \left(A_{\text{p}}^{1/3} + A_{\text{t}}^{1/3}\right)$, and A_{p}, A_{t} are mass numbers of the projectile and the target. In Table 2, the experimental values of the total reaction cross sections and the two-neutron removal cross sections are compared with the data obtained based on the TDSE solution. The obtained two-neutron removal cross sections correspond to experimental data. It can be noted that the total neutron transfer cross section is much smaller than the two-neutron removal cross section. Although, at backward angles, the neutron transfer process has a significant contribution to two-neutron removal probabilities.

Table 2.
The cross-sections for two-neutron removal σ_{-2n} and neutron transfer σ_{tr} channels and the total reaction cross-sections.

E_{lab}	Exp. [12] σ_{-2n}	Theory σ_{-2n}	Theory σ_{tr}	Exp. [12] σ_R
24.3 MeV	5100 mb	4863 mb	105 mb	5400 mb
29.8 MeV	6500 mb	5800 mb	300 mb	7800 mb

Conclusion

The evolution of the probability density and the probability of transfer and breakup were determined based on a numerical solution of the time-dependent Schrödinger equation for outer weakly bound neutrons of the ^{11}Li nucleus. Calculations indicate that at 29.8 MeV, the ^{9}Li yield is greater than at 24.3 MeV due to the greater probability of neutron transfer to the target. Theoretical predictions of the two-neutron removal probability values were obtained for angles from 140° to 180°. The neutron transfer process does not give a large contribution to the total two-neutron removal cross sections, although this is observed for values at backward angels.

Acknowledgement

The authors would like to thank the HybriLIT team (JINR, Dubna, Russia) for the opportunity to use the computational resources of the HybriLIT cluster and support.

This work was supported by the Ministry of Education and Science of the Republic of Kazakhstan within the program of funding research activities through grants for 2018–2020 «Experimental and theoretical research of the interaction of light weakly bound nuclei at low energies – for astrophysical applications» (grant no. 303 of March 29, 2018).

References

[1] K.A. Kuterbekov et al., Chinese Journal of Physics **55** (2017) 2523.
[2] Yu.E. Penionzhkevich et al., Phys. Rev. C **99** (2019) 014609.
[3] A.M. Kabyshev et al., J. Phys. G Nucl. Part. Phys. **45** (2018) 025103.
[4] R.E. Warner et al., Phys. Rev. C **54** (1996) 1700.
[5] L. Chen et al., High Energy Phys. Nucl. Phys. **31** (2007) 1102.
[6] A.C.C. Villari et al., Phys. Lett. B **268** (1991) 345.
[7] A. Lemasson et al., Phys. Rev. Lett. **103** (2009) 232701.
[8] P.G. Hansen et al., Annu. Rev. Nucl. Part. Sci. **45** (1995) 591.
[9] J.S. Vaagen et al., Physica Scripta T **88** (2000) 209.
[10] A.K. Azhibekov et al., Chinese Journal of Physics (2020) doi: 10.1016/j.cjph.2020.01.009.
[11] J.P. Fernandez-Garcia et al., Physical Review Letters **110** (2013) 142701.

[12] J.P. Fernandez-Garcia et al., Physical Review C **92** (2015) 044608.
[13] V.I. Zagrebaev et al., Phys. Rev. C **75** (2007) 035809.
[14] S. Cwiok et al., Computer Physics Communications **46** (1987) 379-399.
[15] A.K. Azhibekov et al., Eurasian Journal of Physics and Functional Materials **3**(4) (2019) 307.
[16] V.V. Samarin, Bull. Russ. Acad. Sci.: Phys. **78** (2014) 1124.
[17] A. Winther, Nucl. Phys. A **572** (1994) 191.
[18] M.E. Riley, B. Ritchie, Phys. Rev. A **59** (1999) 3544.
[19] C. Golabek and C. Simenel, Phys. Rev. Lett. **103** (2009) 042701.